Applied Catalysis B: Environmental 294 (2021) 120252

Contents lists available at ScienceDirect

Applied Catalysis B: Environmental

journal homepage: www.elsevier.com/locate/apcatb

Fouling of TiO_2 induced by natural organic matters during photocatalytic water treatment: Mechanisms and regeneration strategy

Xuejia Yang [a,1], Hongwei Sun [b,1], Guiying Li [a], Taicheng An [a,*], Wonyong Choi [c,*]

[a] Guangdong Key Laboratory of Environmental Catalysis and Health Risk Control, Guangzhou Key Laboratory Environmental Catalysis and Pollution Control, School of Environmental Science and Engineering, Institute of Environmental Health and Pollution Control, Guangdong University of Technology, Guangzhou, 510006, China
[b] Key Laboratory of Pesticide & Chemical Biology of Ministry of Education, Institute of Environmental & Applied Chemistry, College of Chemistry, Central China Normal University, Wuhan, 430079, China
[c] Division of Environmental Science and Engineering, Pohang University of Science and Technology (POSTECH), Pohang, 37673, Republic of Korea

ARTICLE INFO

Keywords:
Photocatalytic water treatment
TiO_2
Humic acid
Catalyst fouling
Advanced oxidation process

ABSTRACT

Photocatalysis has been intensively investigated for the removal of pollutants but little attention was paid to the deactivation of photocatalysts during the long-term operation. Herein we used TiO_2 as the model photocatalyst to investigate its durability in the presence of humic acid (HA), a ubiquitous constituent of real water. No sign of TiO_2 deactivation was observed without HA, whereas significant deactivation occurred with HA. Interestingly, the adsorption of intact HA had only a minor contribution to the deactivation, and the major contributing factor was the adsorption of in-situ oxidized HA, which formed surface complexes with TiO_2, blocked the active sites, and decreased the efficiency of photogenerated charge transfer. The regeneration of the deactivated TiO_2 was also systematically investigated. The present study provides basic information that is required to understand and hinder the complex fouling phenomenon that can be serious in photocatalytic treatment of water containing natural organic matters.

1. Introduction

Photocatalysis for the removal of various environmental pollutants has been a popular research topic in recent decades. In the photocatalytic reaction, the photocatalyst absorbs incident photons of which energy is higher than its bandgap, and generates electrons (e^-) and holes (h^+) [1]. Although most of the charge carriers quickly recombine, a small fraction of them can migrate to the surface of the catalyst and transfer to adsorbed dioxygen and water molecules to form reactive species such as superoxide anion radicals ($^{\bullet}O_2^-$) and hydroxyl radicals ($^{\bullet}OH$), which can degrade and mineralize most organic pollutants. With advantages like mild reaction conditions, simple equipment, less secondary pollution, and utilization of solar light as a sole external energy input, photocatalysis is a promising technique for pollution control [2]. Among various photocatalysts, TiO_2 is the most popular because of its low cost, high activity, good stability and low toxicity [3,4]. However, in practical use, TiO_2 can be deactivated easily [5,6], thus leading to a decrease in pollutant removal efficiency. The need to frequently replace the catalyst increases the cost, thereby limits its wide application. For example, Weon et al. reported the photocatalytic degradation efficiency of toluene with TiO_2 nanotubes decreased from 100 % to 50 % after 200 min [7]. Einaga et al. found that the TiO_2 photocatalytic degradation of benzene decreased from 63 % to 9 % after 120 min [8]. Deactivation of TiO_2 were also reported during the photocatalytic degradation of chlorine-containing volatile organic compounds (Cl-VOCs), ammonia, amines, sulfur-containing pollutants such as H_2S and methyl mercaptan [9–14]. Mechanism studies have shown that the deactivation of the catalyst is related to the adsorption of refractory intermediates of pollutant degradation at the surface active sites, including carbonaceous polymeric substance, chloride, nitrate, sulfate, etc [14–19].

However, most research works on photocatalyst deactivation mainly deal with air-solid photocatalytic reaction systems, and those for water-solid photocatalytic systems have been rarely reported. This might be related with the fact that the photocatalyst deactivation in water is less serious when compared with the cases of gas-phase reactions, since the presence of water as a solvent dissolves out the products and intermediates of pollutants degradation from the photocatalyst surface [20]. However, an important issue we should notice is that most of

---

* Corresponding authors.
E-mail addresses: antc99@gdut.edu.cn (T. An), wchoi@postech.edu (W. Choi).
[1] These authors contribute equally to this work.

https://doi.org/10.1016/j.apcatb.2021.120252
Received 15 November 2020; Received in revised form 19 April 2021; Accepted 20 April 2021

reported photocatalytic reactions in water till now have been conducted in pure water in the absence of any interfering substances. However, real water systems like surface water, groundwater and wastewater, the constituents are generally much more complicated and various species like inorganic ions, natural organic matters (NOMs), biological macromolecular components, and microorganisms are ubiquitous [21], which are likely to cause the deactivation of photocatalysts [22]. For instance, Crittenden et al. found that TiO_2 did not show any deactivation within 25 days of successive photocatalytic operation when used to purify the contaminated groundwater which was pretreated with ion exchange resin to remove the inorganic ions. However, when the raw groundwater was used, TiO_2 was rapidly passivated after only 1 h [23], which demonstrates that various complex components in water can cause the deactivation of photocatalyst. However, our understanding of the deactivation of photocatalysts in real water systems is currently very limited [24].

NOMs are common constituents of surface water, groundwater, wastewater and other water bodies, accounting for 40–80% of the total organic carbon contents in natural waters [25]. In the presence of NOMs, the efficiencies of photocatalytic degradation of target contaminants were reported to be significantly affected [1,26–28], possibly due to the following reasons: (i) NOMs adsorb on the surface of photocatalysts and block the active sites for target pollutants adsorption; (ii) NOMs scavenge the photo-generated reactive species; (iii) NOMs shield the incident light irradiation and reduce the light absorption by photocatalysts [29]. However, we notice that the previous studies were carried out within relatively short time periods of minutes to hours, and the durability of photocatalysts affected by NOMs for longer time (*e.g.,* in repeated batch runs of the recycled photocatalysts) has rarely been investigated in detail. Compared with the instant and temporary impacts of NOMs on photocatalysts, the long-term and accumulative effects of NOMs are of more practical significance, e.g., to help prevent the deactivation either by eliminating the fouling factors or by developing anti-fouling catalysts, as well as to explore regeneration methods of the deactivated photocatalysts.

Therefore, in this study we employed the classical UV/TiO_2 system to investigate the long-term impacts of NOMs on the deactivation of photocatalysts. 2,4,6-trichlorophenol (TCP) was employed as a target pollutant because it is a common aquatic pollutant widely generated in industrial processes producing dye, pesticide, plastics, etc. [30], and has raised concern from the public because of its high bioaccumulation and carcinogenicity [31,32]. Moreover, TCP has relatively simple molecular structure and been widely used as a model substrate to indicate the photocatalytic performance of TiO_2 in different systems for comparison [33,34]. Humic acid (HA) is used as a representative substance of NOMs [35]. The deactivation of TiO_2 was systematically carried out by recycling the batch experiments in the absence and presence of HA. The deactivation mechanism was investigated by studying the adsorption of HA, the transformation of HA, and the characterization of the bulk and surface properties of the deactivated TiO_2. Finally, the deactivated TiO_2 was regenerated using different methods.

2. Experimental section

2.1. Materials

Evonik aeroxide P25 was used as the TiO_2 photocatalyst. 2,4,6-trichlorophenol (TCP) (98 %) and humic acid (HA) (98.2 %) were purchased from J&K Scientific (Beijing, China). Methanol was purchased from ANPEL Laboratory Technology Co. Ltd. (Shanghai, China). Ultrapure water with a resistivity of 18.2 MΩ cm was obtained from an instrument Unique-R20, and all of the materials were used as received without further purification.

2.2. Characterizations

The X-ray diffraction (XRD) patterns of the samples were obtained to characterize the crystal structures of the catalysts using a D/MAX diffractometer (Cu-*K*α radiation). Ultraviolet–visible (UV–vis) diffuse reflectance spectra (DRS) were recorded on a UV–vis spectrophotometer (Cary 300) equipped with an integrating sphere attachment within a range of 200–800 nm and with $BaSO_4$ employed as the internal reflectance standard. X-ray photoelectron spectroscopy (XPS) analysis was performed using a Thermo Fisher Scientific Escalab 250Xi spectrometer that employed monochromatic Al Kα radiation (beam spot size of 650 μm) as the X-ray source and a hemispherical analyzer. The vacuum in the analysis chamber was $< 5.0 \times 10^{-10}$ mbar, and the voltage and current were 15 kV and 15 mA, respectively. All the binding energies were calibrated against the C 1s peak of the surface adventitious carbon at 284.8 eV. The Fourier transformed-infrared spectroscopy (FT-IR) analysis was performed on a NICOLET iS10 FT-IR spectrophotometer at a resolution of 4 cm^{-1} within the range of 400–4000 cm^{-1}. The samples were analyzed using a fluorescence spectrophotometer with a xenon lamp excitation source (F-4600, Hitachi), the three-dimensional excitation emission matrix fluorescence spectroscopy (EEM) was obtained at excitation wavelengths from 200 to 600 nm in 5 nm increments, and emission from 250 to 800 nm in 5 nm increments, with a scan rate of 2400 nm min^{-1}. The Brunauer–Emmett–Teller (BET) specific surface areas and pore size distribution were measured through N_2 adsorption and desorption isotherms with a Micromeritics ASAP 2020 M apparatus.

Photocurrent tests were carried out using a CHI660E electrochemical workstation in a conventional three-electrode system, which were immersed into the solution of 0.5 M Na_2SO_4 (50 mL, pH = 6.5). The ITO/TiO_2 electrodes served as the working electrode, which was prepared on indium-tin oxide (ITO) conductor glass, and 2 mg sample powder was ultrasonicated in 1 mL anhydrous ethanol to form the dispersed solution. The dispersion (50 μL) was then drop-casted onto the ITO glass electrode with a coated area of ca. 1 cm^2. Pt foil and the Ag/AgCl electrode were used as the counter electrode and the reference electrode, respectively. A 300-W Xe lamp was used as an irradiation light source.

2.3. Photocatalytic experiments

Typically, 1 g/L TiO_2 and 200 μM TCP with different concentrations of humic acid was used for the photocatalytic test. The concentration of TCP was within the range of reported TCP concentrations in the industrial wastewater, and the dose of TiO_2 was selected according to those frequently adopted by the literature, also taking into consideration the mass loss of photocatalyst during recycling. The mixed solution was transferred into a 40 mL cylindrical quartz reactor with a diameter of 3 cm, which was mounted in a multi-channel photocatalysis platform (PCX50A, Beijing Perfectlight Co. Ltd.), as shown in Fig. S1. The LED UV lamp with the wavelength centered at around 365 nm was used as the cold-light source for photocatalytic reactions (Fig. S2). The light intensity at the surface of the reaction system was measured to be around 90 mW/cm^2. The internal ventilation system maintained the reacting solution at room temperature during the photocatalytic reaction, and the solution was magnetically stirred at 300 rpm. Samples were taken at predetermined time intervals and filtered, and the filtrate was analyzed for the concentration of TCP by using a high-performance liquid chromatography system (HPLC, Agilent 1260).

For recycling experiments of TiO_2, the suspension after 60 min of photocatalytic reaction was centrifuged at 10,000 rpm for 10 min, and the supernatant solution was carefully removed to minimize the loss of TiO_2. Then, a fresh solution of 200 μM TCP with a given concentration HA was added and mixed thoroughly with the recycled TiO_2 to start the next photocatalysis run. The catalysts after multi-cycle runs were collected and washed with pure water, then dried in a vacuum oven at 60 °C overnight for further characterization. To investigate the impact of TiO_2 loss during recycling on photocatalytic TCP removal, the mass of residual TiO_2 was monitored after 10, 20, 30 and 60 photocatalytic cycles as the control, moreover, different TiO_2 dose was tested for the photocatalytic TCP removal efficiency to evaluate the impact of TiO_2 mass loss.

2.4. Regeneration of deactivated TiO_2 photocatalysts

Three methods were conducted to regenerate the deactivated TiO_2 samples, i.e., ultrasonic washing with alkaline solution, UV regeneration and calcination, respectively. For alkaline washing, 0.04 g deactivated catalyst was dispersed in water, the pH of which was adjusted with 0.1 M NaOH, and then sonicated for different duration to remove the deposited carbon. The catalyst was collected and washed with water before TCP degradation test. UV regeneration was carried out with a multi-band mercury lamp to irradiate the deactivated TiO_2 in pure water at different light intensity and duration. The emission spectrum of the lamp is shown in Fig. S3. In the calcination regeneration procedure, 0.04 g deactivated catalyst was calcined in a Muffle furnace under ambient atmosphere, with the temperature and calcination time optimized. To characterize the activity of the regenerated TiO_2, they were dispersed in 200 μM fresh TCP solution for photocatalytic degradation experiments, and the removal rate of TCP was compared with the fresh TiO_2 to evaluate the regeneration efficiencies of the 3 methods.

3. Results and discussion

3.1. The effect of humic acid on the photocatalysis of TiO_2

To evaluate the impact of NOMs on the durability of TiO_2 during photocatalytic water treatment, HA was adopted as a model NOM in this study. HA apparently promoted the photolysis of TCP in the UV/HA control system (Fig. 1a), due to the well-known role of HA as a photosensitizer to produce reactive oxygen species (ROS) like singlet oxygen ($^1O_2$) for TCP removal [36,37]. In the dark control (TiO_2/HA system), no removal of TCP was observed, suggesting that the presence of HA does not induce the adsorption of TCP on TiO_2 (Fig. 1b). In the UV/TiO_2/HA system, low concentration (5 mg/L) of HA promoted the degradation of TCP, whereas higher [HA] inhibited TCP degradation (Fig. 1c). At low concentrations, HA could act as a photosensitizer (similar to dyes) in the photocatalysis system, i.e., the HA molecules adsorbed on the surface of TiO_2 are photoexcited and subsequently inject electrons to the CB of TiO_2, leading to the ROS generation and pollutant removal [38,39]. The negative effect observed at higher HA concentrations may be due to the light shielding effect of HA and the competitive consumption of ROS by HA itself. To confirm this, the photocatalytic degradation of HA in the TiO_2 suspension was investigated by measuring the UV absorbance at 254 nm [40]. In the absence of TiO_2, only less than 10 % of HA is

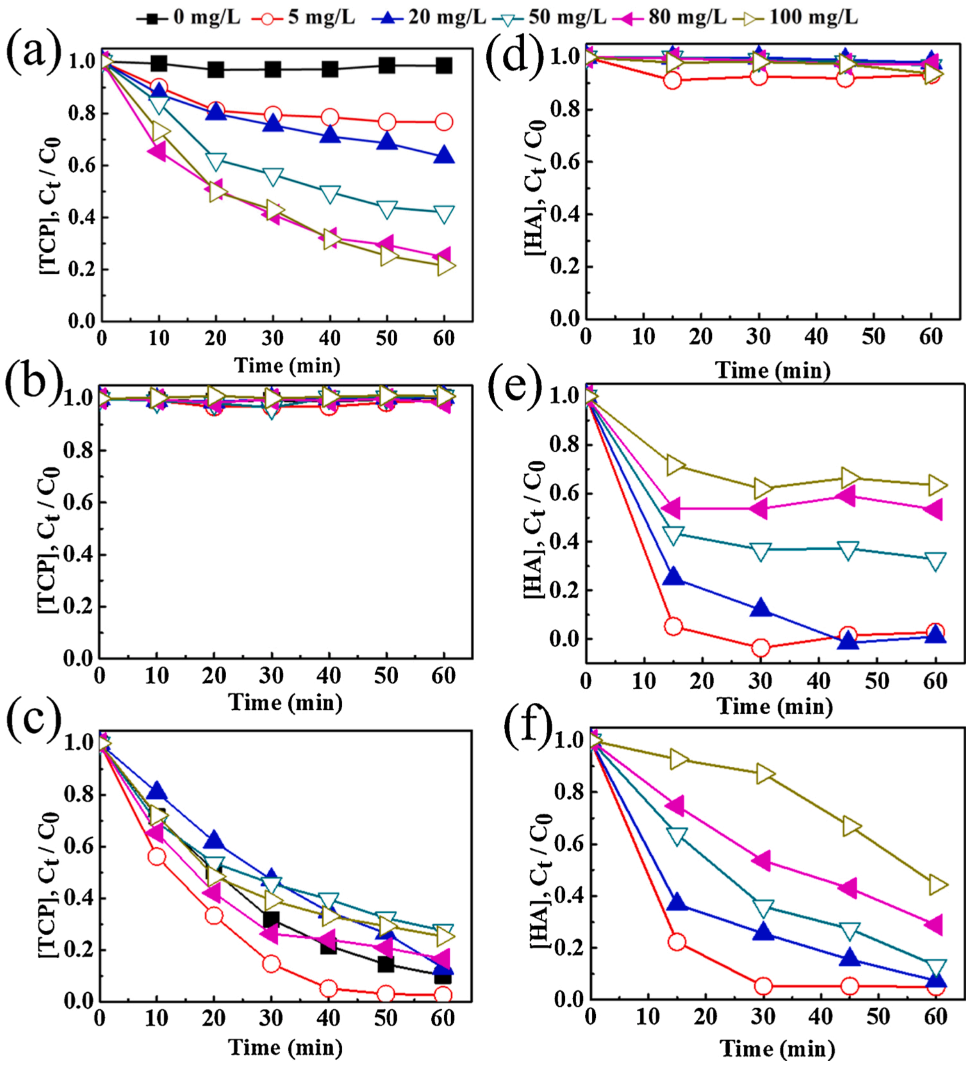

Fig. 1. The time profiles of 2,4,6-TCP removal in (a) UV/HA (b) TiO_2/HA and (c) UV/TiO_2/HA systems. The time profiles of HA removal (monitored by measuring absorbance at 254 nm (A_{254}) in (d) UV/HA, (e) TiO_2/HA, and (f) UV/TiO_2/HA systems. Experimental conditions: $[TCP]_0$ = 200 μM, $[TiO_2]_0$ = 1 g/L, $[HA]_0$ as indicated in the symbol legend.

degraded at [HA] of 5 mg/L and no significant photolysis of HA is observed at higher [HA], suggesting the direct photolysis of HA only contributed slightly to its removal (Fig. 1d). When TiO_2 was added in the dark, HA was efficiently adsorbed on TiO_2 within 1 h, indicating the high affinity of HA to TiO_2 surface, which would facilitate the degradation of HA in the subsequent photocatalytic process (Fig. 1e). As expected, HA concentrations decreased steadily in the UV/TiO_2/HA system, and notably, the rate of HA removal was even faster in the photocatalytic process than those in the dark adsorption, especially in the presence of high concentration HA (Fig. 1f), suggesting that HA was removed by the photocatalytic degradation process, rather than by adsorption. Herein, HA degradation could be attributed to both the electron transfer process and the ROS-induced oxidation processes. Although it is difficult to figure out the exact contribution of the two routes, the TCP degradation profile in Fig. 1c suggested the ROS scavenging effect of HA outweighed its role as a photosensitizer at [HA] $>$ 20 mg/L. Therefore, we concluded that the HA degradation in the photocatalytic process was mainly attributed to the ROS attack, especially at high HA concentrations.

3.2. The deactivation of TiO_2 photocatalyst in the presence of humic acid

We first investigated the reusability of TiO_2 for the photocatalytic removal of TCP in pure water without HA. The direct photolysis of TCP under UV irradiation was less than 5 %, and its adsorption on TiO_2 was also insignificant, but the photocatalytic degradation process removed 100 % of TCP in 60 min. The TiO_2 was then separated and resuspended in a fresh TCP solution to initiate the subsequent photocatalytic cycle. Such process was repeated 60 times (60 min long each run). We found that the photocatalytic performance of the recycled TiO_2 was maintained through the cycles, with more than 95 % of TCP removed at the 60th run using the recycled TiO_2. This indicated the good durability of TiO_2 for photocatalytic removal of organic pollutants in pure water (Fig. 2).

The long-term impact of HA on the durability of TiO_2 during the photocatalytic water treatment was further investigated by using the recycling batch experiments. Photocatalytic degradation of TCP was performed in the presence of different concentrations of HA for 60 min, then TiO_2 particles was recovered by centrifugation and resuspended in a fresh solution of TCP and HA for the next cycle of photocatalysis run. The photocatalytic performance of the TiO_2 catalyst was characterized by monitoring the degradation profile of TCP at the 1st, 10th, 20th and 30th runs. Although there was no sign of TiO_2 deactivation in the absence of HA even after 60 cycles (Fig. 2), the presence of 5 mg/L HA induced the gradual deactivation of TiO_2 after 10 cycles (Fig. 3a), and the deactivation was more severe with higher HA concentrations (Fig. 3b–d). Table S1 indicates clearly that the pseudo first-order rate constant of TCP degradation was little changed after 30 cycles in the absence of HA, whereas it exhibited a marked reduction after 30 cycles in the presence of 5 mg/L HA. Higher concentrations of HA further accelerated the deactivation of TiO_2: the rate constant in the presence of 20 mg/L HA decreased from 0.0525 min^{-1} to 0.0195 min^{-1} after 10 cycles and further to 0.0052 min^{-1} after 30 cycles. According to the literature, the concentration range of dissolved organic matter (DOM) in natural water is 0.3–30 mg/L [37], but 5 mg/L of HA required too many reaction cycles to observe the sign of TiO_2 deactivation, which induced longer experimental time and higher catalyst loss. Therefore, HA of 20 mg/L was chosen for further study in this work.

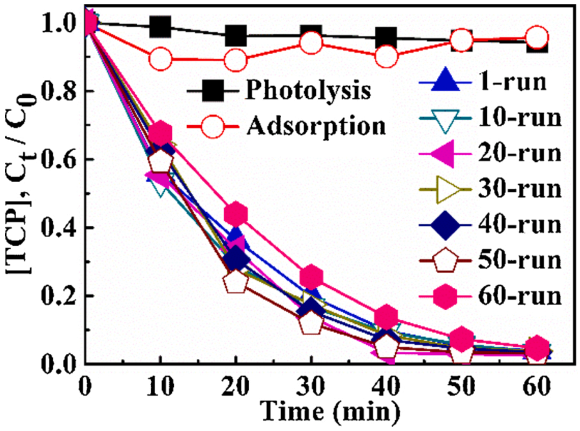

Fig. 2. The photocatalytic activities of TiO_2 for the degradation of TCP in pure water (without HA) during the multi-cycle test. Experimental conditions: $[TCP]_0$ = 200 μM, $[TiO_2]_0$ = 1 g/L.

3.3. Mechanism of TiO_2 deactivation

The TiO_2 samples recovered after different cycles of photocatalysis in the presence of 20 mg/L HA were characterized by XRD, but no significant difference in the XRD patterns was observed with repeating the photocatalysis cycles (Fig. 4a). Similarly, for the recycled TiO_2 in the presence of different HA concentrations, the XRD pattern did not change much except that a sharp new peak appeared at $2\theta = 26°$ in the presence of 100 mg/L HA (Fig. 4b). However, this peak should be attributed to the adsorbed HA according to the fact that a similar XRD peak is observed at this angle for the pure HA sample (Fig. S4). These results suggested that the presence of HA did not induce any significant change of the bulk composition or crystallinity of TiO_2 during the repeated photocatalysis of TCP degradation, therefore, the deactivation of TiO_2 would be related with the change of surface properties.

The gradual deactivation of the irradiated suspended TiO_2 particles in the presence of HA might be caused by several paths. A possible trivial cause of the apparent deactivation of TiO_2 is the gradual loss of TiO_2 mass as the recovery by centrifugation and resuspension of TiO_2 was repeated during the multicycle test. However, considering the fact that the photocatalytic degradation of TCP showed negligible decrease in the absence of HA otherwise under the same experimental condition, the possible contribution of the TiO_2 mass loss to the apparent deactivation can be ruled out. To further confirm this, we conducted the control tests of TCP photocatalytic removal by using different doses of TiO_2, namely 1, 0.75, 0.5 and 0.25 g/L, but the removal efficiency of TCP was little reduced when lowering the TiO_2 content from 1 to 0.25 g/L. This indicates that 1 g/L TiO_2 is high enough for a potential catalyst loss (if any) not to influence the photocatalytic degradation of TCP during recycling experiments (Fig. S5). The mass loss of TiO_2 was also monitored during the recycling experiments. In the absence of HA, TiO_2 concentration decreased to 0.474 g/L after 60 cycles, with the mass loss of 52.63 %, but the TCP degradation only slightly decreased (Fig. 2). In presence of HA, TiO_2 concentration decreased to ca. 0.920, 0.840 and 0.778 g/L after 10, 20 and 30 cycles, corresponding to mass loss of 8 %, 16 % and 22 %, respectively, but the TCP removal rate was reduced by 31 %, 53 %, and 72 %. These results conclude that the contribution of TiO_2 mass loss to the retardation of photocatalytic TCP removal should be negligible.

3.3.1. Effect of adsorbed HA

A plausible cause of the deactivation of TiO_2 is the adsorption of HA on TiO_2 surface, which would lower the photocatalytic performance via shielding irradiation light, blocking the adsorption of target contaminants on the catalyst surface, and the competitive consumption of the photo-generated reactive species. On the basis of the observed adsorption behavior of HA on TiO_2 (Fig. 1e), the long-term adsorption behavior of HA on TiO_2 was tested under the dark condition for 30 h. At [HA] = 5 mg/L, A_{254} decreased quickly to almost 0 within 0.5 h without exhibiting further increase. At higher [HA], A_{254} decreased quickly within the initial 1 h and the adsorption of HA could be saturated within 5 h. Although some fluctuation was observed due to the heterogeneity of HA molecules and the decreased solubility at higher [HA], a trend of equilibrium was reached across the duration of 30 h (Fig. S6). Then, the TiO_2

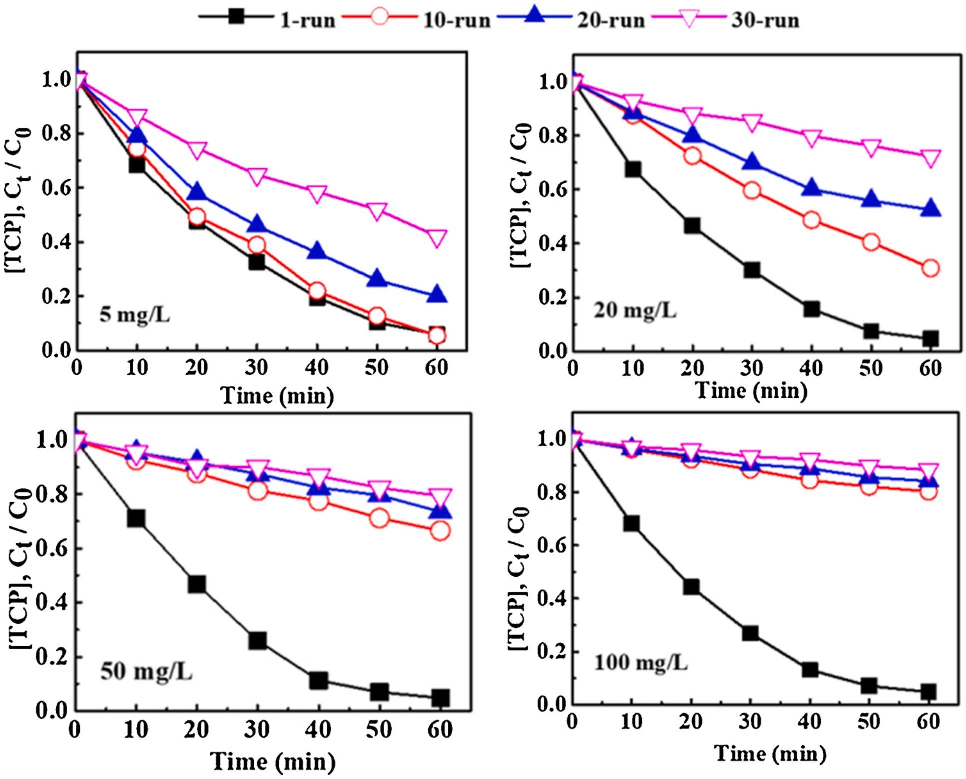

Fig. 3. The gradual deactivation of TiO_2 which was monitored during the repeated cycles of photocatalytic degradation of TCP in the presence of varying concentration of HA, namely (a) 5 mg/L, (b) 20 mg/L, (c) 50 mg/L and (d) 100 mg/L. $[HA]_0$ was maintained constant at the beginning of each run, except at 1st, 10th, 20th, and 30th runs, and the photocatalytic degradation of TCP at 1st, 10th, 20th, and 30th runs was performed in pure water without HA to estimate only the degree of deactivation of TiO_2 without the photosensitization effect of HA. Experimental conditions: $[TCP]_0 = 200$ μM, $[TiO_2]_0 = 1$ g/L.

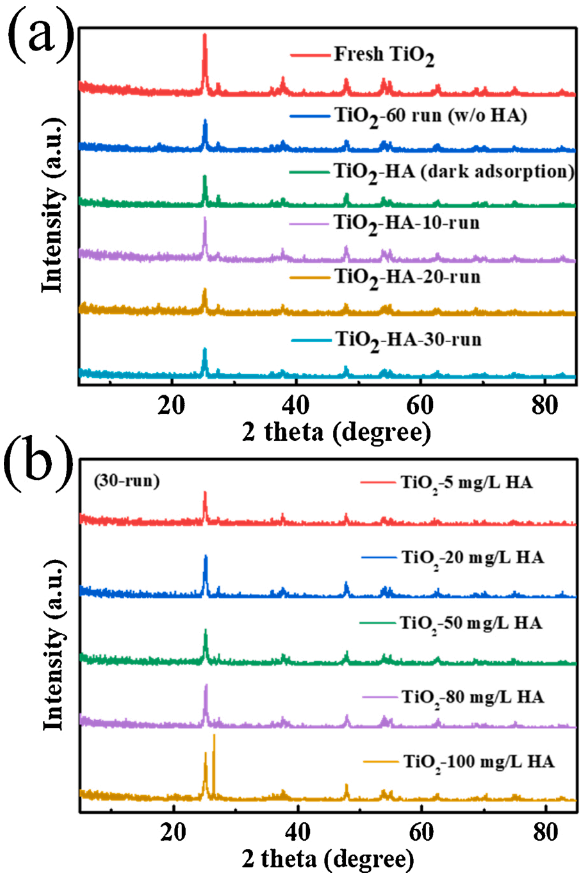

Fig. 4. The XRD pattern of (a) the TiO_2 collected after different cycles of photocatalysis in the presence of 20 mg/L HA, and (b) the TiO_2 collected after 30 cycles of photocatalysis in the presence of different concentrations of HA.

after 30 h of HA pre-adsorption were collected and used for photocatalytic TCP removal. As expected, the photocatalytic performance of the HA-adsorbed TiO_2 was lower than fresh TiO_2, and the higher pre-adsorbed HA concentration resulted in the lower TCP degradation efficiency (Fig. S7). Therefore, the adsorbed HA should contribute to the deactivation of TiO_2 during long-term cycling. Nonetheless, when compared with the recycling photocatalysis experiments, the extent of deactivation caused by HA adsorption alone was far less. For example, in the presence of 20 mg/L HA, the adsorption of HA caused 20 % decrease of the pseudo first-order rate constant of TCP removal, much lower than that (91.5 %) caused by 30 cycles of photocatalysis in the presence of the same concentration HA (Tables S1 and S2). These results indicate that the adsorption of HA should be a minor factor of the TiO_2 deactivation, the major cause of which remains unidentified.

3.3.2. *Role of surface deposited species*

We subsequently characterized the surface property of the deactivated TiO_2 (after 30 photocatalytic cycles with 20 mg/L of HA) by using SEM and EDS elementary mapping technique (Fig. S8). EDS analysis indicates that the surface of the deactivated TiO_2 mainly composed of Ti, O, C and N, accounting for 30.7 %, 58.2 %, 7.7 % and 3.1 % by atomic percentage, respectively (Fig. S8c), with the spatial distribution of C and N in good accordance with Ti and O. Large quantity of carbon and nitrogen content is ascribed to the adsorbed HA molecules or their transformation byproducts.

We then carefully examined the XPS spectra of the TiO_2 before and after deactivation. The intensities of the Ti 2p bands centered at 458.4 and 464 eV (assigned to Ti-O) decreased gradually during recycling with HA (Fig. 5a), and a similar trend was observed with the O 1s band at 529.6 eV (lattice O, Fig. 5b), possibly due to the shielding of surface Ti and O atoms by the adsorbed organic matter after repeated use. Moreover, it is noteworthy that the Ti 2p and O 1s bands of the TiO_2 samples shifted toward higher binding energy (B.E.) after deactivation in the presence of HA (Fig. 5a and b). To better show the B.E. shift of Ti 2p and O 1s bands during the recycled photocatalysis, the B.E. shift values were

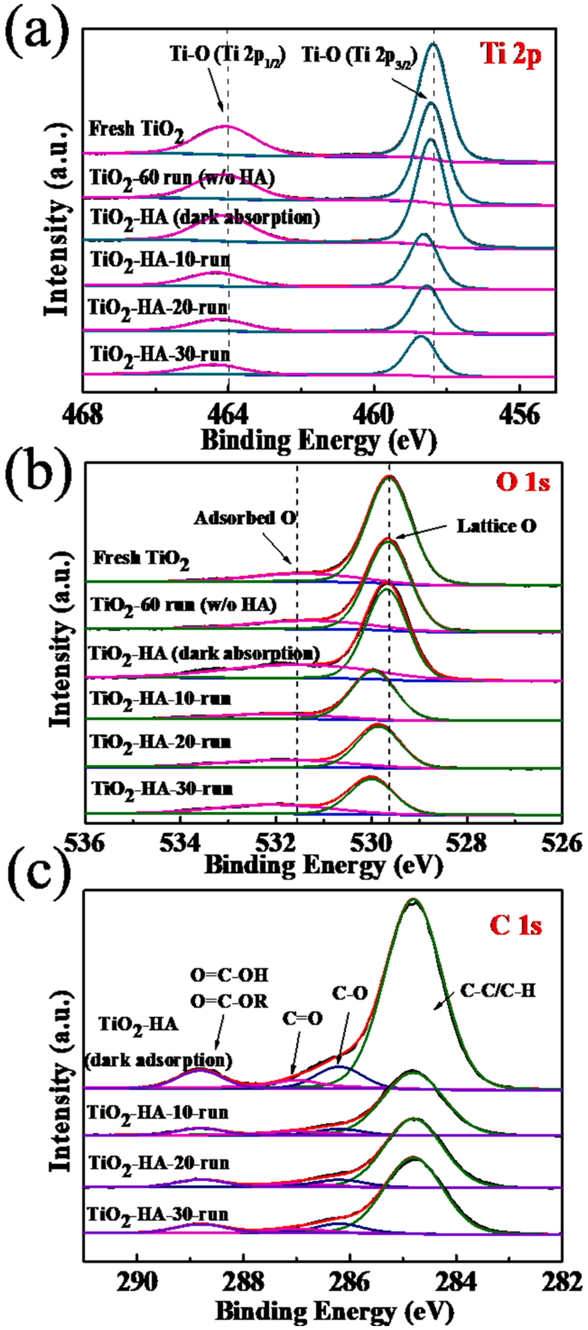

Fig. 5. The X-ray photoelectron spectra (XPS) of (a) Ti 2p, (b) O 1s, and (c) C 1s bands for the TiO_2 sample reacted with HA.

calculated and listed in Table S3 (The B.E. values in fresh TiO_2 were used as the reference and its B.E. shift was 0 eV). In the HA dark adsorbed TiO_2 sample, the B.E. of Ti 2p and O 1s slightly shifted, whereas all the peaks including Ti $2p_{3/2}$, Ti $2p_{1/2}$, lattice oxygen and the adsorbed oxygen shifted toward larger B.E. values after the recycled photocatalytic experiments, and the B.E. shift increased with the number of recycles. This might be due to the formation of surface complexes between the adsorbed HA and TiO_2. However, since we did not observe such B.E. shift or the intensity decrease in the control samples (TiO_2 after 60 cycles w/o HA and TiO_2 after dark HA adsorption), the B.E. shift in the HA-deactivated TiO_2 should be attributed to the adsorption of oxidized HA byproducts. They could form surface complexes with the lattice Ti and O atoms on TiO_2 surface, e.g., the carboxyl groups were reported to have strong affinity to TiO_2 nanoparticles, and could form bidentate complexes with the surface Ti atoms [38,41,42]. The surface complexing ligands withdraw the electron density from the surface Ti and O atoms, inducing the positive B.E. shift of Ti 2p and O 1s. Obviously, HA molecules would undergo oxidative transformation in the photocatalytic reaction, generating more oxygen-containing groups and facilitating the chemisorption of HA byproducts on TiO_2 [43,44]. To confirm, the C 1s spectra of the TiO_2 samples after HA dark adsorption and photocatalytic recycling was deconvoluted according to the methods for humic substance reported by the literature [45–49]. Results showed that the proportion of C—C/C—H (284.8 eV) decreased after photocatalytic recycling, with the simultaneous increase of the oxygen-containing groups, including C—O (286.2 eV), C═O (287.8 eV) and O═C—OH/O═C—OR (289.0 eV) (Fig. 5c and Table S4). These results corroborate the coverage of TiO_2 surface by oxidized HA, which might be recalcitrant to further photocatalytic degradation and lead to the deactivation of TiO_2.

It was reported that deposited heteroatoms such as Cl and N species (e.g., Cl^-, nitrate and ammonia) are responsible for the deactivation of TiO_2 during the photocatalytic removal of volatile organic compounds [14], so we tried to characterize Cl and N elements in the used TiO_2 with XPS analysis. When the photocatalytic degradation of TCP was recycled in absence of HAs, only a very weak Cl 2p signal was detected between B.E. value of 196–199 eV in the TiO_2 after 60 cycles (Figs. S9a and b), and no Cl 2p signal was observed in the XPS of TiO_2 after 30 cycles in presence of HA (Fig. S9c), suggesting that Cl impurity was not responsible for the deactivation of TiO_2. In addition, weak N 1s signals were detected in the TiO_2 samples after both HA dark adsorption and recycled photocatalysis with HA (Fig. S10a), but regarding our experiments were conducted in water and the high solubility of nitrate and ammonia. The detected N 1s signals were probably not assigned to the inorganic nitrogen species, but stem from the organic nitrogen contained in HA molecules, as supported by the similar N 1s spectra between fresh HA (Fig. S10b) and the deactivated TiO_2 samples.

As we showed that the adsorption of HA alone accounted for a minor part of the deactivation, the adsorption of oxidized HA on TiO_2 may be responsible for its deactivation. To characterize the transformation of HA, we examined the FT-IR spectra of different TiO_2 samples (Fig. 6). The FT-IR spectrum of the original HA was similar with that reported in the literature [48,49], and the major absorbance bands and their assignments are summarized in Table S5. After adsorption on TiO_2, the details of HA spectrum below 1200 cm^{-1} were shielded by the strong absorption of TiO_2, and notably, new peaks emerged at 3850, 2620 and 1860 cm^{-1}, possibly caused by the formation of surface complex between TiO_2 and the HA moieties like —OH and —COOH, but the exact assignment of these IR peaks is not clear at this moment. The TiO_2 after 60 cycles of photocatalytic removal of TCP without HA showed two sharp peaks at 1230 and 1160 cm^{-1}. The peak at 1160 cm^{-1} is the characteristic of the CH_2 vibration in $(CH_2)_n$-$(COOH)_2$, and the band at 1230 cm^{-1} is attributed to the hydroquinone (1,2-HQ or 1,4-HQ) according to the literature [50]. These results indicated that TCP underwent oxidation processes, resulting in the cleavage of the aromatic rings and the formation of carboxylic groups, which facilitated their adsorption on the TiO_2 through the surface coordination pathways. However, in the presence of HA, the intensity of the peaks at 1230 and 1160 cm^{-1} (regarded as the indicators of TCP byproducts adsorbed on the TiO_2) decreased with recycling times, accompanied by the increasing peaks at 3850, 2620 and 1860 cm^{-1} (the characteristics of HA adsorbed on TiO_2), which indicated that the oxidized HA showed higher adsorption affinity to the surface of TiO_2 than the TCP byproducts, therefore causing the deactivation of TiO_2 for photocatalytic TCP removal.

N_2 adsorption-desorption isotherm was then measured to determine the effect of HA byproducts adsorption on the pore structure and surface area of TiO_2. All samples exhibited type-IV isotherms with hysteresis loops, indicating the existence of mesoporous structure of the P25 TiO_2 (Fig. S11). The S_{BET}, pore volume and average pore size of fresh TiO_2 were 55.2 $m^2\ g^{-1}$, 0.4 $cm^3\ g^{-1}$ and 14.8 nm, respectively. After 60 cycles

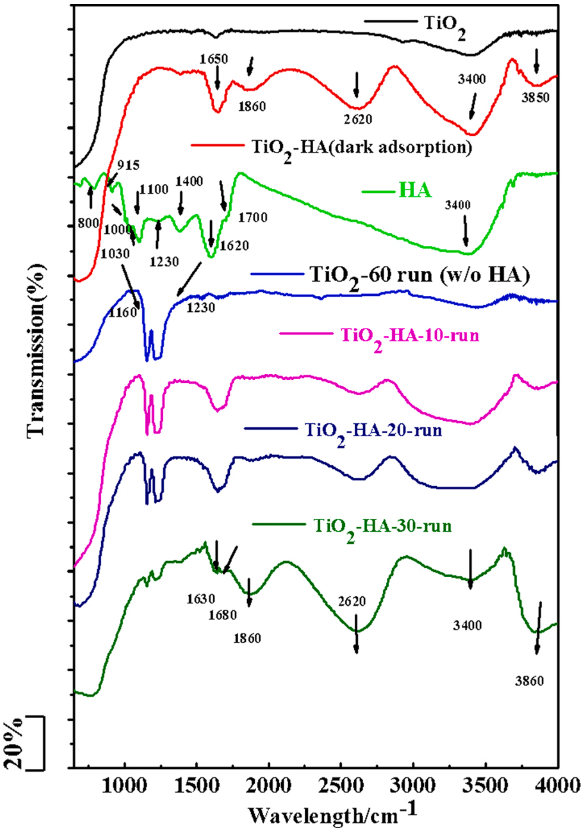

Fig. 6. The FI-IR spectra of the control samples including fresh TiO_2, original HA and the HA-adsorbed TiO_2, and the TiO_2 collected after photocatalytic recycling experiments. Experimental conditions: $[TiO_2]_0 = 1$ g/L, $[TCP]_0 = 200$ μM, $[HA]_0 = 20$ mg/L.

without HA, the S_{BET}, pore volume and average pore size decreased to 48.4 m^2 g^{-1}, 0.4 cm^3 g^{-1} and 14.4 nm, respectively. These parameters showed slight decrease after HA dark adsorption, but reduced to 48.3 m^2 g^{-1}, 0.3 cm^3 g^{-1} and 14.0 nm when cycled for 30 runs in presence of HA (Table S6), suggesting that the adsorbed HA byproducts blocked some pores of the TiO_2, which could also contribute to the deactivation of TiO_2. The diffuse reflectance spectra (DRS) of the deactivated TiO_2 were also measured. The light absorption of the TiO_2 samples in the visible-light region (> 400 nm) increased with repeating the photocatalytic cycles in the presence of HA (Fig. 7a), which was also apparent from the dark color of TiO_2 samples (see the photo images in Fig. 7a). The increased absorbance in the visible region should be attributed to the adsorbed HA content which is believed to form surface complex with TiO_2. On the other hand, the photocurrent response obtained with the photocatalyst-coated electrode was markedly reduced with the recycled TiO_2-HA samples, whereas the photocurrent of the recycled TiO_2 without HA showed no sign of decline (Fig. 7b). Therefore, the decreased photocurrent should be caused by the adsorbed HA, which shields the incident light and scavenges the photogenerated charges on the surface of TiO_2.

The deactivated TiO_2 was further characterized by using the TGA technique, and the results indicated that the mass loss was not significant for the fresh TiO_2 up to the temperature of 800 °C, although some transformation of the crystal phase of TiO_2 should take place within this temperature range [51]. However, the HA-induced deactivated TiO_2 samples showed obvious mass loss between 400 °C–600 °C, and the mass loss increased with more recycled samples (Fig. 7c). This suggests that more oxidized HA adsorbs on TiO_2 with increasing the photocatalysis cycles, and subsequently occupies more surface sites with causing gradual deactivation of TiO_2. Interestingly, although the mass losses (>6 %) of the TiO_2 after 60 cycles without HA (with TCP alone) was comparable with that of the deactivated TiO_2 after 10 cycles with HA, no sign of deactivation was observed without HA. This indicates that the deactivation level is not directly correlated with the mass of carbonaceous deposits on TiO_2, whereas the chemical species of the deposited carbon matters.

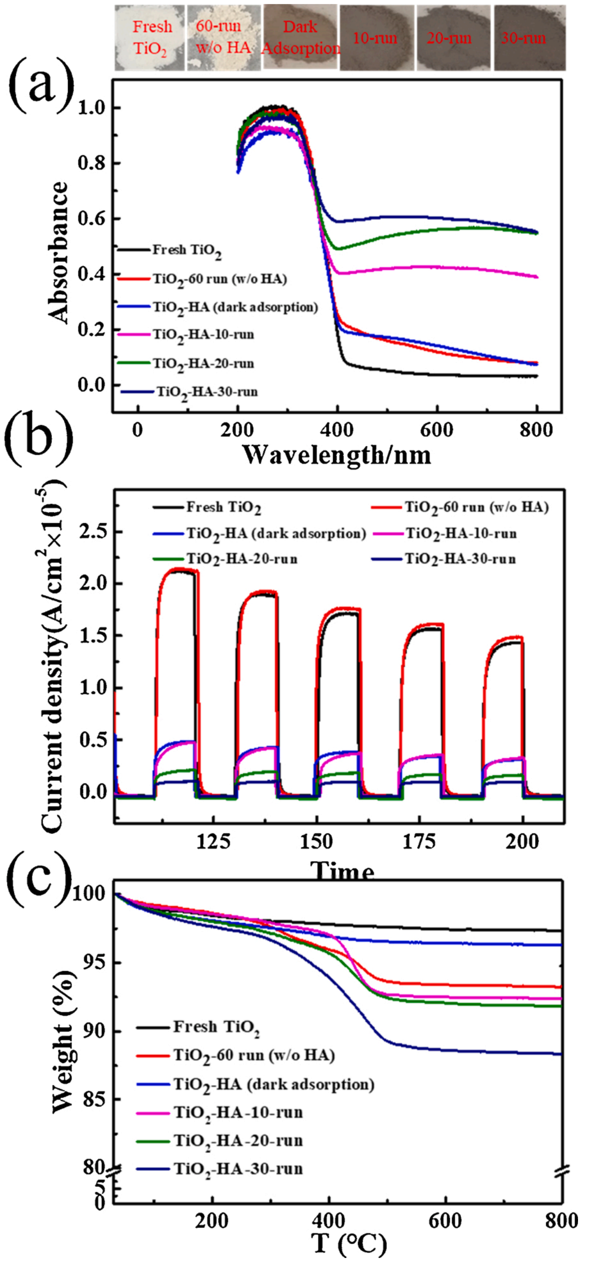

Fig. 7. (a) The UV–vis diffuse reflectance spectra (DRS) of fresh and deactivated TiO_2. (b) The photocurrent-time profiles of the fresh and deactivated TiO_2 electrode under UV light irradiation (c) The thermal gravimetric analysis (TGA) patterns of the fresh and deactivated TiO_2, TGA was conducted under air atmosphere. On the top of this chart showed the photographs of different TiO_2 samples.

We further washed the deactivated TiO_2 with alkaline solution to collect the oxidized byproducts of HA that were chemisorbed on the photocatalyst surface for better characterization. However, after the elute was freeze-dried, the amount of the recovered solute was too small for FTIR test. Instead, we analyzed the elute solution with EEM. The elute from HA dark adsorbed TiO_2 sample showed the typical fluorescent peak of humic substance at excitation (Ex)/emission (Em) of 260 nm/460 nm [52,53], and notably, the fluorescent intensity of the elute decreased gradually with repeating the photocatalytic cycles although fresh HA was supplemented for each photocatalytic cycle (Fig. 8). This suggests the fluorophores such as the aromatic rings and the Π conjugated structures of the adsorbed HA on TiO_2 surface were steadily destructed by the photocatalytic process, producing non-fluorescent byproducts. These results provide a solid proof to our hypothesis that the deactivation of TiO_2 is not induced by the adsorbed HA molecules, but their oxidized byproducts.

3.4. Catalyst regeneration strategy

The regeneration of the deactivated photocatalyst is important in real water treatment applications, from the viewpoint of cost control [54]. In this study, we demonstrated that the adsorption of NOMs (HA) and their transformation byproducts is an important cause of deactivation of TiO_2, therefore, it is essential to remove these adsorbed substances for the regeneration of TiO_2. Herein, we tested several methods to recover the photocatalytic activity of the HA-deactivated TiO_2 (Fig. 9). Since the solubility of the humic-like substance is generally higher at higher pH, we used alkaline solution (pH adjusted with NaOH) to wash the deactivated TiO_2 with the aid of sonication, and the washed TiO_2 was tested for the photocatalytic degradation of TCP. The pseudo first-order rate constants of TCP degradation were obtained to evaluate the efficiencies of the regeneration method (Table S7). As expected, the activity of the TiO_2 was recovered to ca. 84 % of the fresh TiO_2 at the optimal regeneration condition of pH 10.5–11 and ultrasonication of 50 min (Fig. 9a and b). The deactivated TiO_2 was also regenerated by mercury lamp illumination, the parameters including the power of the light source and the illuminating time were optimized, and the photocatalytic activity could be recovered to ca. 45 % of the fresh TiO_2 at the optimal conditions of 700 W (53.8 mW/cm^2) and 6 h (Fig. 9c and d). Thermal treatment was employed as well to regenerate the deactivated catalysts since the carbonaceous deposits could be combusted at high temperature under oxygen atmosphere. Herein, after thermal treatment at 500 °C under air for 30 min, the photocatalytic activity of the deactivated TiO_2 could be restored to ca. 78 % of the fresh TiO_2 (Fig. 9e and f). Compared with alkaline washing and calcination, UV-illumination method was less effective and time-consuming for the regeneration of the deactivated photocatalyst, therefore is not preferred.

4. Conclusion

The fouling of photocatalyst in real water treatments seriously limits its practicality, which needs in-depth investigation and understanding of the fouling mechanism induced by natural water constituents like NOMs. We found that TiO_2 is resistant to deactivation during the repeated cycles of photocatalytic degradation of TCP in pure water, but undergoes gradual deactivation when HA is present in the aqueous suspension of photocatalyst. The adsorption of original HA molecules on the surface of TiO_2 is found to be only a minor cause of the deactivation, and the major contributing factor appears to be the adsorption of HA degradation byproducts during photocatalysis. These byproducts form strongly-bound surface complexes with the TiO_2 surface, which subsequently block the active sites of the photocatalyst with inducing the deactivation of TiO_2. On the other hand, the TiO_2 photocatalyst that was recovered and reused in the absence of HA exhibited little sign of deactivation for the photocatalytic degradation of TCP. The critical factor that induces the catalyst deactivation seems to be closely related with the chemical speciation of the deposited carbonaceous substances, which is supported by various characterization results of the deactivated TiO_2. It seems that the photocatalytic transformation of HA induces the formation of surface-binding byproducts that deactivate the photocatalyst. The deactivated TiO_2 can be effectively regenerated by alkaline

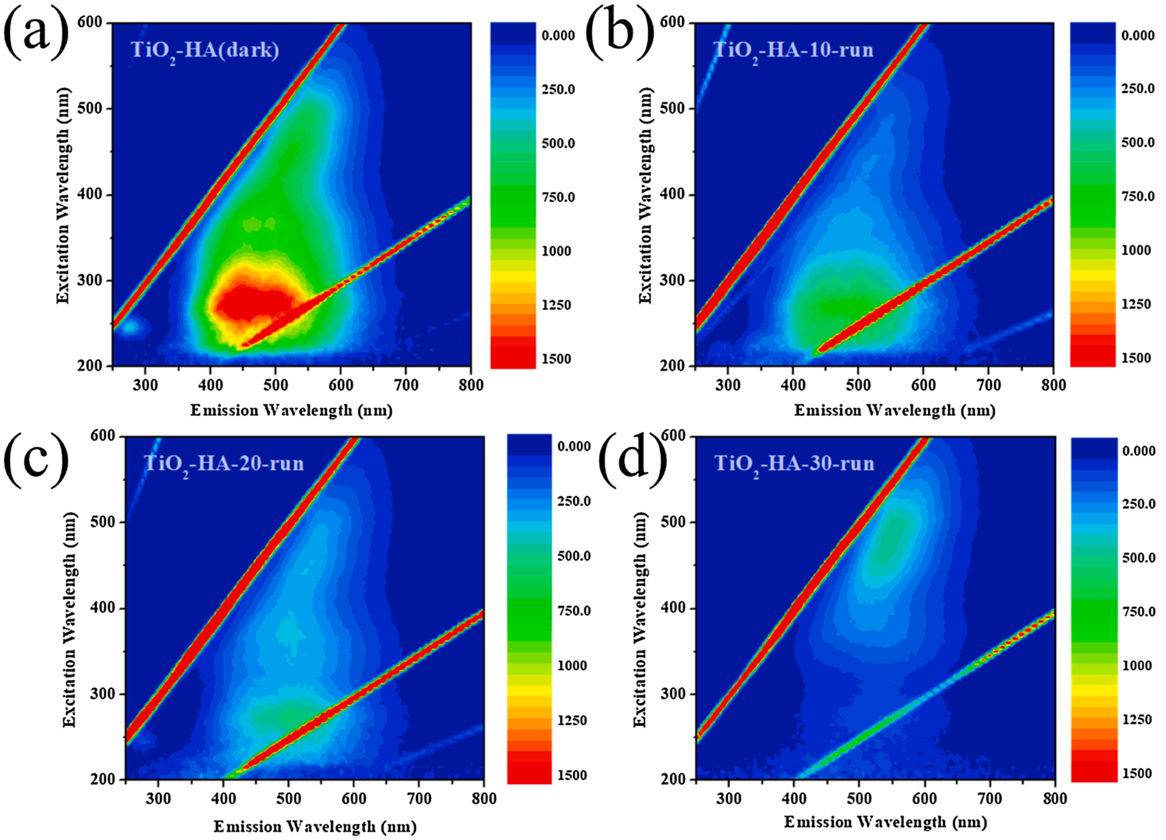

Fig. 8. EEM spectra of the desorbed HA matters from different TiO_2 samples using alkaline washing. (a) TiO_2 after HA dark adsorption, and (b, c, d) TiO_2 after different photocatalytic recycling experiments as indicated on the graph panels.

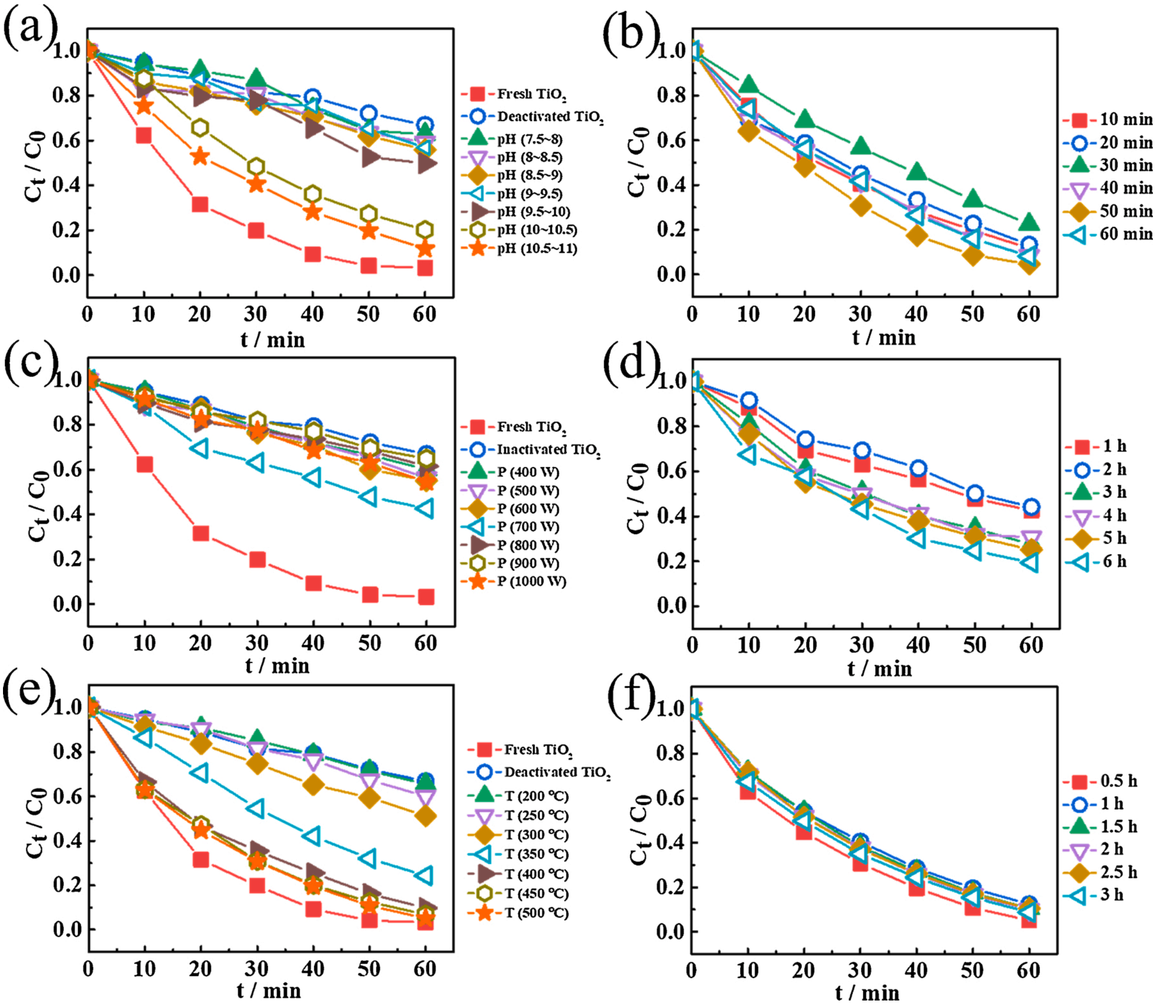

Fig. 9. The photocatalytic TCP degradation performance of the TiO_2 regenerated by different methods, including alkaline washing (a) at different pH for 10 min and (b) at pH = 10.5-11 for different duration; UV light irradiation with the mercury lamp (c) at different power for 1 h and (d) at 700 W for different duration; High temperature calcination (e) at different temperature for 30 min and (f) at 500 °C for different duration. The deactivated TiO_2 refers to the TiO_2 after 10 cycles of photocatalysis with 100 mg/L HA.

washing or thermal treatment. This work provides the detailed information of photocatalyst deactivation process in the presence of natural organic matters in water, which has been rarely investigated despite the extensive studies on photocatalytic water treatment.

Author statement

Xuejia Yang: Methodology, Formal analysis, Writing - original draft.
Hongwei Sun: Investigation, Validation, Writing - original draft.
Guiying Li: Writing - Reviewing and Editing.
Taicheng An: Conceptualization, Supervision.
Wonyong Choi: Conceptualization, Supervision.

Declaration of Competing Interest

The authors declare that they have no known competing financial interests or personal relationships that could have appeared to influence the work reported in this paper.

Acknowledgements

This work was financially supported by National Natural Science Foundation of China (22076030, 41425015, 22076061), and Local Innovative and Research Teams Project of Guangdong Pearl River Talents Program (2017BT01Z032). The financial support from GDUT for Prof. Choi's visit is also appreciated.

Appendix A. Supplementary data

Supplementary material related to this article can be found, in the online version, at doi:https://doi.org/10.1016/j.apcatb.2021.120252.

References

[1] T.E. Doll, F.H. Frimmel, Photocatalytic degradation of carbamazepine, clofibric acid and iomeprol with P25 and Hombikat UV100 in the presence of natural organic matter (NOM) and other organic water constituents, Water Res. 39 (2005) 403–411, https://doi.org/10.1016/j.watres.2004.09.016.

[2] Y.A. Ilan, G. Czapski, D. Meisel, The one-electron transfer redox potentials of free radicals. I. The oxygen/superoxide system, Biochim. Biophys. Acta 430 (1976) 209–224, https://doi.org/10.1016/0005-2728(76)90080-3.

[3] H. Park, H.I. Kim, G.H. Moon, W. Choi, Photoinduced charge transfer processes in solar photocatalysis based on modified TiO_2, Energy Environ. Sci. 9 (2016) 411–433, https://doi.org/10.1039/c5ee02575c.

[4] H. Park, Y. Park, W. Kim, W. Choi, Surface modification of TiO_2 photocatalyst for environmental applications, J. Photochem. Photobiol. C Photochem. Rev. 15 (2013) 1–20, https://doi.org/10.1016/j.jphotochemrev.2012.10.001.

[5] C.H. Bartholomew, Mechanisms of catalyst deactivation, Appl. Catal. A Gen. 212 (2001) 17–60, https://doi.org/10.1016/s0926-860x(00)00843-7.

[6] P. Forzatti, L. Lietti, Catalyst deactivation, Catal. Today 52 (1999) 165–181, https://doi.org/10.1016/s0920-5861(99)00074-7.

[7] S. Weon, E. Choi, H. Kim, J.Y. Kim, H.J. Park, S.M. Kim, W. Kim, W. Choi, Active {001} facet exposed TiO_2 nanotubes photocatalyst filter for volatile organic

compounds removal: from material development to commercial indoor air cleaner application, Environ. Sci. Technol. 52 (2018) 9330–9340, https://doi.org/10.1021/acs.est.8b02282.

[8] H. Einaga, S. Futamura, T. Ibusuki, Heterogeneous photocatalytic oxidation of benzene, toluene, cyclohexene and cyclohexane in humidified air: comparison of decomposition behavior on photoirradiated TiO_2 catalyst, Appl. Catal. B Environ. 38 (2002) 215–225, https://doi.org/10.1016/S0926-3373(02)00056-5.

[9] M. Hegedus, A. Dombi, Gas-phase heterogeneous photocatalytic oxidation of chlorinated ethenes over titanium dioxide: perchloroethene, Appl. Catal. B Environ. 53 (2004) 141–151, https://doi.org/10.1016/j.apcatb.2004.05.010.

[10] H.H. Ou, S.L. Lo, Photocatalysis of gaseous trichloroethylene (TCE) over TiO_2: the effect of oxygen and relative humidity on the generation of dichloroacetyl chloride (DCAC) and phosgene, J. Hazard. Mater. 146 (2007) 302–308, https://doi.org/10.1016/j.jhazmat.2006.12.039.

[11] Q.J. Geng, Q.J. Guo, C.Q. Cao, Y.C. Zhang, L.T. Wang, Investigation into photocatalytic degradation of gaseous ammonia in CPCR, Ind. Eng. Chem. Res. 47 (2008) 4363–4368, https://doi.org/10.1021/ie800274g.

[12] R. Portela, B. Sanchez, J.M. Coronado, R. Candal, S. Suarez, Selection of TiO_2-support: UV-transparent alternatives and long-term use limitations for H_2S removal, Catal. Today 129 (2007) 223–230, https://doi.org/10.1016/j.cattod.2007.08.005.

[13] T. Sano, K. Koike, T. Hori, T. Hirakawa, Y. Ohko, K. Takeuchi, Removal of methyl mercaptan with highly-mobile silver on graphitic carbon-nitride (g-C_3N_4) photocatalyst, Appl. Catal. B Environ. 198 (2016) 133–141, https://doi.org/10.1016/j.apcatb.2016.05.057.

[14] F. He, U. Muliane, S. Weon, W. Choi, Substrate-specific mineralization and deactivation behaviors of TiO2 as an air-cleaning photocatalyst, Appl. Catal. B Environ. 275 (2020) 119145, https://doi.org/10.1016/j.apcatb.2020.119145.

[15] K. Demeestere, J. Dewulf, H. Van Langenhove, Heterogeneous photocatalysis as an advanced oxidation process for the abatement of chlorinated, monocyclic aromatic and sulfurous volatile organic compounds in air: state of the art, Crit. Rev. Environ. Sci. Technol. 37 (2007) 489–538, https://doi.org/10.1080/10643380600966467.

[16] S. Weon, W. Choi, TiO_2 nanotubes with open channels as deactivation-resistant photocatalyst for the degradation of volatile organic compounds, Environ. Sci. Technol. 50 (2016) 2556–2563, https://doi.org/10.1021/acs.est.5b05418.

[17] J. Chen, Z. He, Y. Ji, G. Li, T. An, W. Choi, OH radicals determined photocatalytic degradation mechanisms of gaseous styrene in TiO_2 system under 254 nm versus 185 nm irradiation: combined experimental and theoretical studies, Appl. Catal. B Environ. 257 (2019) 117912, https://doi.org/10.1016/j.apcatb.2019.117912.

[18] M. Wen, G. Li, H. Liu, J. Chen, T. An, H. Yamashita, Metal–organic framework-based nanomaterials for adsorption and photocatalytic degradation of gaseous pollutants: recent progress and challenges, Environ. Sci. Nano 6 (2019) 1006–1025, https://doi.org/10.1039/C8EN01167B.

[19] P. Yao, H. Liu, D. Wang, J. Chen, G. Li, T. An, Enhanced visible-light photocatalytic activity to volatile organic compounds degradation and deactivation resistance mechanism of titania confined inside a metal-organic framework, J. Colloid Interf. Sci. 522 (2018) 174–182, https://doi.org/10.1016/j.jcis.2018.03.075.

[20] L.Q. Jing, B.F. Xin, F.L. Yuan, B.Q. Wang, K.Y. Shi, W.M. Cai, H.G. Fu, Deactivation and regeneration of ZnO and TiO_2 nanoparticles in the gas phase photocatalytic oxidation of n-C_7H_{16} or SO_2, Appl. Catal. A Gen. 275 (2004) 49–54, https://doi.org/10.1016/j.apcata.2004.07.019.

[21] H. Shi, G. Li, H. Sun, T. An, H. Zhao, P.K. Wong, Visible-light-driven photocatalytic inactivation of E. Coli by Ag/AgX-CNTs (X=Cl, Br, I) plasmonic photocatalysts: bacterial performance and deactivation mechanism, Appl. Catal. B Environ. 158-159 (2014) 301–307, https://doi.org/10.1016/j.apcatb.2014.04.033.

[22] H.U. Farouk, A.A.A. Raman, W.M.A.W. Daud, TiO_2 catalyst deactivation in textile wastewater treatment: current challenges and future advances, J. Ind. Eng. Chem. 33 (2016) 11–21, https://doi.org/10.1016/j.jiec.2015.10.022.

[23] J.C. Crittenden, Y. Zhang, D.W. Hand, et al., Solar detoxification of fuel-contaminated groundwater using fixed-bed photocatalysts, Water Environ. Res. 68 (1996) 270–278, https://doi.org/10.2175/106143096X127703.

[24] H. Shi, J. Chen, G. Li, X. Nie, H. Zhao, P.-K. Wong, T. An, Synthesis and characterization of novel plasmonic Ag/AgX-CNTs (X = Cl, Br, I) nanocomposite photocatalysts and synergetic degradation of organic pollutant under visible light, ACS Appl. Mater. Inter. 5 (2013) 6959–6967, https://doi.org/10.1021/am401459c.

[25] M. Erhayem, M. Sohn, Stability studies for titanium dioxide nanoparticles upon adsorption of Suwannee River humic and fulvic acids and natural organic matter, Sci. Total Environ. 468 (2014) 249–257, https://doi.org/10.1016/j.scitotenv.2013.08.038.

[26] R. Enriquez, P. Pichat, Interactions of humic acid, quinoline, and TiO_2 in water in relation to quinoline photocatalytic removal, Langmuir 17 (2001) 6132–6137, https://doi.org/10.1021/la010599w.

[27] C. Lin, K.S. Lin, Photocatalytic oxidation of toxic organohalides with TiO_2/UV: the effects of humic substances and organic mixtures, Chemosphere 66 (2007) 1872–1877, https://doi.org/10.1016/j.chemosphere.2006.08.027.

[28] C.X. Zhang, Y.X. Wang, Effects of dissolved organic matter in landfill leachate on photodegradation of environmental endocrine disruptors, Int. J. Environ. Pollut. 45 (2011) 69–80, https://doi.org/10.1504/ijep.2011.039086.

[29] A. Katz, A. McDonagh, L. Tijing, H.K. Shon, Fouling and inactivation of titanium dioxide-based photocatalytic systems, Crit. Rev. Environ. Sci. Technol. 45 (2015) 1880–1915, https://doi.org/10.1080/10643389.2014.1000763.

[30] M.Z. Khan, P.K. Mondal, S. Sabir, Bioremediation of 2-chlorophenol containing wastewater by aerobic granules-kinetics and toxicity, J. Hazard. Mater. 190 (2011) 222–228, https://doi.org/10.1016/j.jhazmat.2011.03.029.

[31] A.J. Batik, P.R. Gogate, Hybrid treatment strategies for 2,4,6-trichlorophenol degradation based on combination of hydrodynamic cavitation and AOPs, Ultrason. Sonochem. 40 (2018) 383–394, https://doi.org/10.1016/j.ultsonch.2017.07.029.

[32] R. Xu, J. Cui, R. Tang, F. Li, B. Zhang, Removal of 2,4,6-trichlorophenol by laccase immobilized on nano-copper incorporated electrospun fibrous membrane-high efficiency, stability and reusability, Chem. Eng. J. 326 (2017) 647–655, https://doi.org/10.1016/j.cej.2017.05.083.

[33] F. Li, P. Du, W. Liu, X. Li, H. Ji, J. Duan, D. Zhao, Hydrothermal synthesis of graphene grafted titania/titanate nanosheets for photocatalytic degradation of 4-chlorophenol: Solar-light-driven photocatalytic activity and computational chemistry analysis, Chem. Eng. J. 331 (2018) 685–694, https://doi.org/10.1016/j.cej.2017.09.036.

[34] A. Shoneye, J. Tang, Highly dispersed FeOOH to enhance photocatalytic activity of TiO_2 for complete mineralisation of herbicides, Appl. Surf. Sci. 511 (2020) 145479, https://doi.org/10.1016/j.apsusc.2020.145479.

[35] K. Yang, D. Lin, B. Xing, Interactions of humic acid with nanosized inorganic oxides, Langmuir 25 (2009) 3571–3576, https://doi.org/10.1021/la803701b.

[36] D. Vione, G. Falletti, V. Maurino, C. Minero, E. Pelizzetti, M. Malandrino, R. Ajassa, R.I. Olariu, C. Arsene, Sources and sinks of hydroxyl radicals upon irradiation of natural water samples, Environ. Sci. Technol. 40 (2006) 3775–3781, https://doi.org/10.1021/es052206b.

[37] M.J. Zhan, X. Yang, Q.M. Xian, L.G. Kong, Photosensitized degradation of bisphenol A involving reactive oxygen species in the presence of humic substances, Chemosphere 63 (2006) 378–386, https://doi.org/10.1016/j.chemosphere.2005.08.046.

[38] W. Wu, G. Shan, Q. Xiang, Y. Zhang, S. Yi, L. Zhu, Effects of humic acids with different polarities on the photocatalytic activity of nano-TiO_2 at environment relevant concentration, Water Res. 122 (2017) 78–85, https://doi.org/10.1016/j.watres.2017.05.010.

[39] H. Zheng, Z. Wang, J. Zhao, S. Herbert, B. Xing, Sorption of antibiotic sulfamethoxazole varies with biochars produced at different temperatures, Environ. Pollut. 181 (2013) 60–67, https://doi.org/10.1016/j.envpol.2013.05.056.

[40] I. Sutzkover-Gutman, D. Hasson, R. Semiat, Humic substances fouling in ultrafiltration processes, Desalination 261 (2010) 218–231, https://doi.org/10.1016/j.desal.2010.05.008.

[41] W. Chen, C. Qian, X.Y. Liu, H.Q. Yu, Two-dimensional correlation spectroscopic analysis on the interaction between humic acids and TiO_2 nanoparticles, Environ. Sci. Technol. 48 (2014) 11119–11126, https://doi.org/10.1021/es502502n.

[42] J. Balajka, M.A. Hines, W.J.I. DeBenedetti, M. Komora, J. Pavelec, M. Schmid, U. Diebold, High-affinity adsorption leads to molecularly ordered interfaces on TiO_2 in air and solution, Science 361 (2018) 786–788, https://doi.org/10.1126/science.aat6752.

[43] D. Chen, Z. Jiang, J. Geng, Q. Wang, D. Yang, Carbon and nitrogen co-doped TiO_2 with enhanced visible-light photocatalytic activity, Ind. Eng. Chem. Res. 46 (2007) 2741–2746, https://doi.org/10.1021/ie061491k.

[44] K. Yang, B. Xing, Sorption of phenanthrene by humic acid-coated nanosized TiO_2 and ZnO, Environ. Sci. Technol. 43 (2009) 1845–1851, https://doi.org/10.1021/es802880m.

[45] W. Chen, H. Wang, Q. Gao, Y. Chen, S. Li, Y. Yang, D. Werner, S. Tao, X. Wang, Association of 16 priority polycyclic aromatic hydrocarbons with humic acid and humin fractions in a peat soil and implications for their long-term retention, Environ. Pollut. 230 (2017) 882–890, https://doi.org/10.1016/j.envpol.2017.07.038.

[46] F. Yang, S. Zhang, K. Cheng, M. Antonietti, A hydrothermal process to turn waste biomass into artificial fulvic and humic acids for soil remediation, Sci. Total Environ. 686 (2019) 1140–1151, https://doi.org/10.1016/j.scitotenv.2019.06.045.

[47] J. Jia, Y. Zhang, Q. Liu, G. Huang, B. Xing, C. Zhang, H. Guo, J. Pan, Y. Cao, Characterization of coal-based humic acids in relation to their preparation methods, Energy Sources Part A Recovery Util. Environ. Eff. (2020) 1–11, https://doi.org/10.1080/15567036.2020.1824034.

[48] G. Huang, Z. Xiao, W. Zhen, Y. Fan, C. Zeng, C. Li, S. Liu, P.K. Wong, Hydrogen production from natural organic matter via cascading oxic-anoxic photocatalytic processes: an energy recovering water purification technology, Water Res. 175 (2020) 115684, https://doi.org/10.1016/j.watres.2020.115684.

[49] F. Monteil-Rivera, E.B. Brouwer, S. Masset, Y. Deslandes, J. Dumonceau, Combination of X-ray photoelectron and solid-state C-13 nuclear magnetic resonance spectroscopy in the structural characterisation of humic acids, Anal. Chim. Acta 424 (2000) 243–255, https://doi.org/10.1016/s0003-2670(00)01139-9.

[50] J. Bandara, J.A. Mielczarski, A. Lopez, J. Kiwi, 2. Sensitized degradation of chlorophenols on iron oxides induced by visible light - Comparison with titanium oxide, Appl. Catal. B Environ. 34 (2001) 321–333, https://doi.org/10.1016/s0926-3373(01)00225-9.

[51] D.A.H. Hanaor, C.C. Sorrell, Review of the anatase to rutile phase transformation, J. Mater. Sci. 46 (2011) 855–874, https://doi.org/10.1007/s10853-010-5113-0.

[52] G.O. Bosire, J.C. Ngila, Assessment of photo-oxidative alterations to natural organic matter in water using fluorescence excitation emission matrices and liquid

chromatography-organic carbon detection techniques, Anal. Methods 8 (2016) 1415–1424, https://doi.org/10.1039/c5ay02086g.

[53] W. Chen, P. Westerhoff, J.A. Leenheer, K. Booksh, Fluorescence excitation - Emission matrix regional integration to quantify spectra for dissolved organic matter, Environ. Sci. Technol. 37 (2003) 5701–5710, https://doi.org/10.1021/es034354c.

[54] X. Pan, N. Zhang, X. Fu, Y.-J. Xu, Selective oxidation of benzyl alcohol over TiO_2 nanosheets with exposed {001} facets: catalyst deactivation and regeneration, Appl. Catal. A Gen. 453 (2013) 181–187, https://doi.org/10.1016/j.apcata.2012.12.023.